J. Fluid Mech. (1988), *vol.* 188, *pp.* 437–464
Printed in Great Britain

Simulation of free boundaries in flow systems by lattice-gas models

By P. CLAVIN,
Laboratoire de Recherche en Combustion, Centre de St Jérôme,
13397 Marseille Cedex 13, France

P. LALLEMAND, Y. POMEAU
Laboratoire de Physique de l'Ecole Normale Supérieure,
24 rue Lhomond 75231 Paris Cedex 05, France

AND G. SEARBY
Laboratoire de Recherche en Combustion, Centre de St Jérôme,
13397 Marseille Cedex 13, France

(Received 30 October 1986 and in revised form 14 August 1987)

It has been recently proved that lattice-gas models with Boolean particles can provide a very powerful method to study viscous flows at moderate Reynolds and small Mach numbers (d'Humières, Pomeau & Lallemand 1985; Frisch, Hasslacher & Pomeau 1986; d'Humières & Lallemand 1986). We present here algorithms for an extension of these models to provide a simple and efficient way to simulate a large variety of flow problems with free boundaries. This is done by introducing two different types of particles that can react following a specific kinetic scheme based on autocatalytic reactions. In order to check the powerful character and the reliability of the method we also present preliminary results of two-dimensional computer simulations concerning problems ranging from the competition between molecular diffusion and turbulent mixing in flows presenting a Kelvin–Helmholtz instability to the spontaneous generation of turbulence in premixed flame fronts subject to the Darrieus–Landau instability. The dynamics of an interface developing a Rayleigh–Taylor instability is also considered as well as some typical problems of phase transition such as spinodal decomposition and the nucleation process.

1. Introduction

The behaviour of large assemblies of atoms or molecules is described by the laws of continuum mechanics (such as the Navier–Stokes equation for normal fluids) in which the discrete nature of the particles has been more or less forgotten. This remark has recently proved to be quite helpful in a proposal for a new method of numerical computation of the equations of fluid mechanics (d'Humières, Pomeau & Lallemand 1985; Frisch, Hasslacher & Pomeau 1986). It consists of representing explicitly in the computation a very simple microscopic world described by a lattice-gas model. This model, which is derived from a model studied earlier (Hardy & Pomeau 1972; Hardy, Pomeau & de Pazzis 1973; and Hardy, de Pazzis & Pomeau 1976), presents the same properties as a normal fluid for large space and time scales. Moreover, because of its discrete character, the lattice-gas model can be handled by a deterministic cellular automaton which may proceed in a massively parallel way.

The preliminary results that have been obtained on one-phase flows at moderate Reynolds numbers are very encouraging (d'Humières *et al.* 1985; d'Humières & Lallemand 1986). For the moment it is probably too early to judge the success of this new method compared to more classical ones improved by years of effort, although the advent of specialized highly parallel computers based on this idea may open new horizons, in particular from the point of view of computational speed. Among the advantages of this approach are the simplicity and the flexibility of the software.

The purpose of this paper is to extend these ideas to the representation of situations in which the dynamics of interfaces are coupled to fluid motion. Typical examples are provided by molecular mixing and chemical reactions developing together in turbulent mixing layers, flames in premixed gas flows and two-phase flows with immiscible fluids or with equilibrium liquid–vapour interfaces. This is noteworthy for being a source of tough problems in computational fluid mechanics. Different possibilities will be presented for describing such interface dynamics with a similar simpified microscopic representation of the continuum. The general method consists in adding a label (such as A or B) to the fluid particles of the lattice gas. This label makes it possible to distinguish between the particles on either side of the interface but particles of a given family (A or B) remain indistinguishable. We shall introduce various models depending on whether or not the label has its own dynamics controlled by a chemical reaction, and whether or not the fluid motion is influenced by the dynamics of the interface.

In each section of the paper, a discrete molecular model for a physical system with an interface will be presented and its elementary properties studied so as to make each section as self-contained as possible. Finally a practical implementation will be proposed and some preliminary results of computer gedanken experiments will also be presented. A brief description of the lattice-gas method is given in Appendix A.

In §2 it will be shown how to model the convection of a completely passive scalar. This corresponds, for instance, to mixing layers as often visualized by differential colouring of the two fluids.

In §3 we shall consider a model in which the labels have non-trivial dynamics leading to the spontaneous formation of thin interfaces. The labels (and thus the interface) are convected by the fluid, but the interface has no influence on the flow field. Each particle bears one of the two possible labels but, contrary to the model presented in §2, this label may change during the course of time. The microscopic laws controlling this 'chemical reaction' are such that particles with the same label tend to be together. The corresponding macroscopic effect leads to a stable phase separation with a thin interface between pools of A and B which coexist forever when the equilibrium conditions for label transformation are satisfied by the microscopic laws. For other conditions, the growth of a stable phase into a metastable or an unstable one can be observed. These models could be helpful for studying nucleation phenomena or chemical reactions in flows.

In §3 we also present a model in which the two labels correspond to states of different internal energy of the fluid particles. Thus label transformations now are subject to a constraint of energy conservation. This constraint is satisfied by coupling the label change to the spin flipping of a dynamical Ising model with its own energy-conserving dynamics. Such a model is useful for crystal growth.

In §4 we outline some of the problems related to the representation of two-phase flows of immiscible or reacting fluids. At the microscopic level, phase separation in real immiscible fluids is related to the balance between repulsive and attractive

molecular forces. It is difficult to implement attractive forces in the discrete lattice gas. It may be noticed, however, that the equilibrium interface between two phases of a substance can be a fair representation of a passive interface between the two immiscible fluids, showing that immiscibility is not necessarily needed at the molecular level. This is the case for phases having the same mechanical properties as the two immiscible fluids whenever the flow-induced perturbations to the local thermodynamic equilibrium on both sides of the interface have a relatively negligible effect upon the motion of this interface. With this in mind, we discuss the conditions for which the interface models of §3 are reasonable approximations to describe front instabilities such as Rayleigh–Taylor or Kelvin–Helmholtz instabilities. In fact, those interfaces behave as thin reaction–diffusion layers so that such models could be also helpful to study the development of chemical reactions in turbulent flows.

Section 5 is devoted to the presentation of a microscopic model in which 'chemical reactions' act on the fluid motion because of temperature and density changes. This is useful for modelling premixed flames. In this model the labels correspond to different states of internal energy of the particles and conservation of energy in label-changing collisions is now ensured by exchanging kinetic energy ($\equiv$ translational) and internal energy. This is made possible by particles having one of two possible non-zero moduli for their microscopic velocities. We shall also present preliminary results of a numerical simulation of this model in which plane flame fronts appear, followed by a time-dependent distortion of the fronts due to the growth of the hydrodynamic instability of Darrieus–Landau.

2. Simple mixing of a passive scalar

There are two ways to represent the behaviour of fluids: Eulerian and Lagrangian. In the Lagrangian approach one follows the trajectories of particles convected by the fluid and it is possible to obtain a direct answer to questions related to dynamical mixing. To give an example of this, as well as a possible way to study it by lattice-gas dynamics, let us consider mixing in a free shear layer. This layer can be obtained experimentally by merging two parallel flows with different velocities. A Kelvin–Helmholtz instability develops and mixes the two fluids in a region of non-potential flow. This mixing phenomenon is basically non-diffusive (Roshko 1967) and can be understood as follows: at the molecular level the thickness of the interface between the two fluids grows as $(Dt)^{\frac{1}{2}}$, where D is the molecular diffusivity and t is the time elapsed since the merging of the two layers, $t = z/u, z$ being the streamwise distance to the merging point, and u the mean flow velocity. However, the typical length for the Kelvin–Helmholtz instability is z. Thus for $z \gg D/u = z_c$ all scales are presumably present in the interface geometry from z down to z_c, so that the interface looks like a fractal with a small-scale cutoff at z_c.

To simulate this in lattice-gas computations, one could think of the following 'gedanken computer experiment'. Using a silicon wind tunnel such as the one presented by d'Humières (d'Humières *et al.* 1985; d'Humières & Lallemand 1986), inject particles of lattice gas with different flow velocities into two parallel jets with two different labels or 'colours'.

This requires, at most, to double the number of bits, since beyond knowing whether a particle is present with a given velocity one also needs to know the 'colour' of the particle. For example, fourteen bits can be used at each site of a hexagonal lattice: six bits show the presence or absence of a particle with a given orientation of the velocity (the modulus of the velocity is the same for all directions); one bit is

for the presence or the absence of a particle at rest; seven bits are used to show the 'colour'.

In the following, the first seven bits will be called the 'hydrodynamic bits' and the seven others the 'colour bits'. Among the 2^{14} corresponding possibilities, only 3^7 represent possible states of a given site. This is because a colour bit has a meaning only when the corresponding hydrodynamic state is occupied. The collisions laws are represented by a table of 3^7 elements determining the correspondence between states before and after collisions. It may be convenient to introduce more than one table, in particular to describe the possibility of collisions having different outlets for a given inlet. Two at least are required to ensure isotropy, see Appendix A. In order to make the colour a truly passive marker in the sense of seeding in experimental tomography (Boyer 1980), these collision tables must be constructed in such a way that the mapping obtained when attention is restricted to the subset associated with the seven hydrodynamic bits corresponds to that given by the tables of 2^7 elements used to describe the ordinary one-phase flow as in d'Humières *et al.* (1985), d'Humières & Lallemand (1986). When the total number of particles, momentum and energy are conserved in the collision rules for the hydrodynamic bits, it can be shown that the Navier–Stokes equations are verified at the macroscopic level (Frisch *et al.* 1986). The collision laws for the colour bits must be such that the number of particles of a given colour is conserved and care must be taken to maintain isotropy and detailed balance. The binary diffusion process and 'random walk' are ensured by the coloured collisions and the validity of Fick's law can be proved following developments similar to those of Frisch *et al.* (1986) and of Rivet & Frisch (1986). However it should be noticed that the hole–particle symmetry present in the original hexagonal model (Frisch *et al.* 1986) is lost when the colour of particles is considered.

In figure 1(a,b) we present the values of the binary diffusion coefficient D of different values of the density as obtained by direct simulations of the lattice-gas algorithm. In these figures (as in the rest of this paper) every dimensionless quantity is expressed in the natural units of the lattice gas: the unit of length is the distance between sites and the unit of time is the corresponding transit time. Note, however, that the density d is expressed in particles per direction per site; the mass density is thus given by $\rho = 7d$. These data have been obtained for two different configurations. The first series of experiments concern the amplitude relaxation of a sinusoidal perturbation in the mass fraction, as in forced Rayleigh diffusion experiments. The exponential decay and the dependence of the relaxation time on the square of the wavelength are found to be well verified, see figure 1(c,d). In the second series of experiments, an initial Heaviside step function in the profile of the densities is allowed to evolve and is fitted with the corresponding error function. The values obtained in the two configurations are equal to within an accuracy of few percent and show that the product of the binary diffusion coefficient and the density is only weakly dependent on the density, as predicted by the kinetic theory of gases.

This extension of the lattice-gas method is convenient to study phenomena in which molecular diffusion and turbulent mixing are present, as in the above-mentioned experiments concerning mixing layers. It is easy to imagine a computer experiment in which one does the same measurements as in real experiments: measure the mean colour in the mixed flow, track the interface and measure its length or area per unit volume, or eventually its fractal dimension. Lines of emission and particle paths can also be easily imaged by this method. The limitation of this model is the same as the one met when studying large-Reynolds-number flows. At

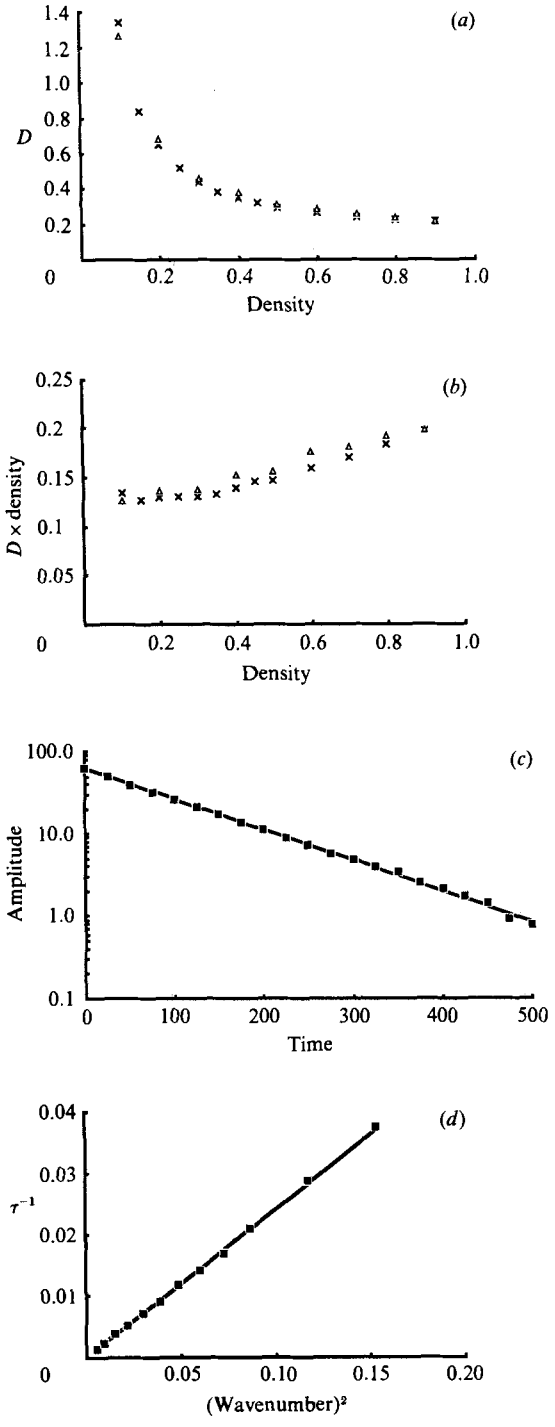

FIGURE 1. (*a*) Binary diffusion coefficient as a function of density. The crosses are obtained from the relaxation of a Heaviside step function, the triangles from an initial sinusoidal perturbation. (*b*) Binary diffusion coefficient times density as a function of density. (*c*) Amplitude of an initial sinusoidal perturbation as a function of time; density = 0.9, $\lambda = 64$. (*d*) Wavenumber-squared dependence of the inverse relaxation time for sinusoidal perturbations; density = 0.8: ——, calculations; ■, experiments.

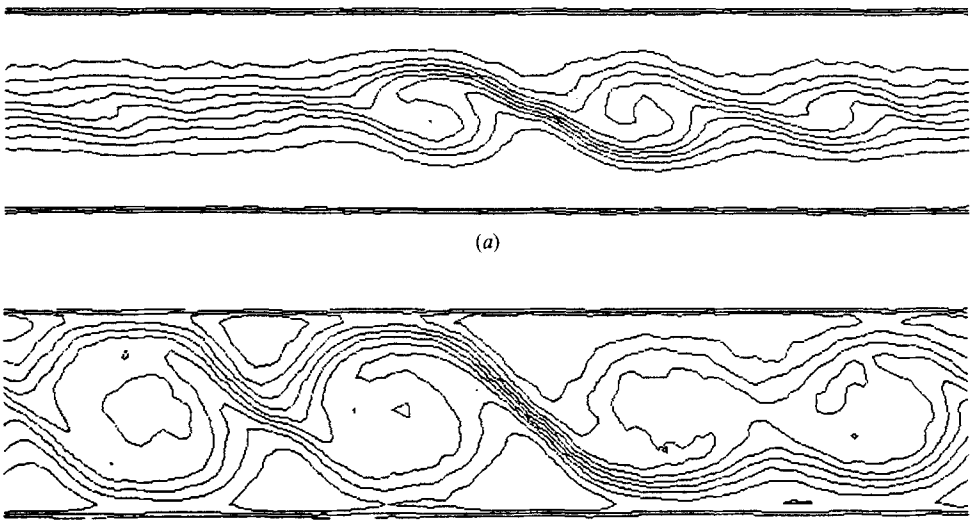

(a)

(b)

FIGURE 2. Turbulent mixing in a Kelvin–Helmholtz instability. (a) time = 2000, (b) 4000.

low density the Schmidt number is of order unity for the lattice gas (it is easy to anticipate this by analogy with a real gas) and the dimensionless ratio z/z_c is thus of the same order of magnitude as the Reynolds number.

Some preliminary results of a computer simulation of the Kelvin–Helmholtz instability developing on a idealized mixing layer are presented in figure 2. A lattice gas of 1024 sites by 256 sites is used in a two-dimensional channel with stick conditions at the upper and lower boundaries and periodic conditions at the ends. The initial condition consists of two symmetric flow regions occupying the upper and lower halves of the channel. The two regions have opposed velocity vectors with the same modulus of $\frac{3}{7}$. This corresponds to a Mach number of $M \approx 0.65$, a Reynolds number based on the width of the box of $Re \approx 330$ and a Schmidt number $D/\nu \approx 1.17$. Molecular diffusion and turbulent mixing proceed as the time goes on to approach the complete equilibrium constituted by a quiescent medium with uniform species concentrations. The pictures after 2000 and 4000 times steps are presented in figure 2. Coherent structures are visualized here by isoconcentration lines.

To study and visualize the dynamics of large structures as well to isolate the turbulent mixing mechanism, it could be interesting to suppress the molecular diffusion process between the two different coloured particles as for the interface between two immiscible fluids. This problem is presented in §4.

3. Interfaces associated with reaction–diffusion waves developing in flows

Equilibrium interfaces may appear between two steady stable states of a system of diffusive particles with autocatalytic reactions. The multiplicity of chemical equilibrium states and their possible coexistence result from the specific properties of the kinetic model (see (1) below) and this is not representative of ordinary chemical systems. By modifying the reaction rates it is also possible to describe the propagation of a near-equilibrium interface associated with the transformation of a metastable state into a stable one. The analogy with the thermodynamics of a first-order phase transition is shown in the equilibrium equations which are very similar

to the ones governing the spatial dependence of the order parameter in the theory of Cahn & Hilliard (1959).

Consider a reacting mixture of particles A and B with the following kinetics:

$$\left.\begin{aligned} A+A+B &\underset{k_A^-}{\overset{k_A^+}{\rightleftharpoons}} A+A+A, \\ B+B+A &\underset{k_B^-}{\overset{k_B^+}{\rightleftharpoons}} B+B+B, \end{aligned}\right\} \tag{1}$$

where $k_{A,B}(>0)$ are the constants of reaction. The corresponding reaction–diffusion equation is

$$\frac{\partial X}{\partial t} = D\Delta X + \omega(X), \tag{2}$$

where X is the mass fraction of A, D the binary diffusion coefficient and ω the reaction rate:

$$\omega = k_A^+ X^2(1-X) + k_B^-(1-X)^3 - k_A^- X^3 - k_B^+ X(1-X)^2. \tag{3}$$

As a first example consider the symmetrical case:

$$\left.\begin{aligned} k_A^+ &= k_B^+ = k^+, \\ k_A^- &= k_B^- = k^-. \end{aligned}\right\} \tag{4}$$

ω is an odd function of $(X-\frac{1}{2})$. When $\kappa = k^-/k^+ < \frac{1}{3}$, it has three real roots X_1, X_2 and $\frac{1}{2}$, ($X_2 = 1-X_1$, in this symmetrical case, $0 < X_{1,2} < 1$), collapsing to $\frac{1}{2}$ for the critical case $\kappa = \frac{1}{3}$. For $\kappa < \frac{1}{3}$, the mass fractions X_1 and X_2 are those of the stable stationary (equilibrium) states. The stationary state $X = \frac{1}{2}$ is unstable for $\kappa < \frac{1}{3}$ but stable and unique otherwise. For non-zero values of $\kappa(<\frac{1}{3})$, both equilibrium states consist of a mixture of A and B with fluctuations in the concentration X. For the particular case $k^- = 0$ ($\kappa = 0$), the two equilbrium states consist of a pure fluid of A ($X = 1$) or of B ($X = 0$) and the reaction rate is

$$\omega = \tfrac{1}{2}k^+ X(1-X)(X-\tfrac{1}{2}). \tag{5}$$

Thus, when κ is smaller than $\frac{1}{3}$, the model may describe the equilibrium between two phases separated by a planar interface, the structure of which is described by the equation

$$D\frac{\mathrm{d}^2X}{\mathrm{d}\xi^2} + \omega = 0, \tag{6a}$$

where ξ is the coordinate normal to the front. When the medium is at rest, there exists an equilibrium position for the interface which depends on the boundary conditions. The thickness δ of the interface is of order

$$\delta \approx \left(\frac{D}{k}\right)^{\frac{1}{2}}, \tag{6b}$$

where k is the frequency factor of the reactive collisions. As in the Cahn & Hilliard theory, the diffusion coefficient D for the order parameter X determines a surface energy. As we shall see in more detail later, this phenomenon controls the diffusive part of the motion of wrinkled interfaces and is responsible for the stability of planar interfaces against accidental wrinkles produced by initial perturbations. It also produces shrinking of initial convex pockets of one species imbedded in the other.

Notice that (2) derives from a Landau–Ginzburg potential:

$$\frac{\partial x}{\partial t} = -\frac{\delta f}{\delta x} \tag{7a}$$

with
$$f = \iiint \{\tfrac{1}{2}D(\nabla x)^2 + W(x)\}\,\mathrm{d}^3 r, \quad \omega = -\frac{\partial W}{\partial x}; \tag{7b}$$

the first term in the bracket corresponds to an interfacial energy.

Consider now a non-symmetrical case (representative of the generic case):

$$k_{\mathrm{A}}^{+} > k_{\mathrm{B}}^{+}, \quad k_{\mathrm{A}}^{-} = k_{\mathrm{B}}^{-} = 0 \tag{8a}$$

(this last condition is used to simplify the presentation and could be replaced by a more general one). In this case the steady state $X = X_1 = 1$ is the most stable case, although $X = X_2 = 0$ is metastable because $W(X_1) < W(X_2)$. Thus, (2) has a unique one-dimensional travelling-wave solution describing the replacement of particles B by A with a wave velocity U corresponding to a nonlinear eigenvalue, in the sense of Barrenblatt & Zeldovich (1972), of the following problem:

$$\left.\begin{aligned} U\frac{\mathrm{d}X}{\mathrm{d}\xi} - D\frac{\mathrm{d}^2 X}{\mathrm{d}\xi^2} &= \omega(x), \\ \xi = -\infty \quad (X = 0); \quad \xi &= +\infty \quad (X = 1). \end{aligned}\right\} \tag{8b}$$

When the imbalance is small, $|k_{\mathrm{A}}^{+} - k_{\mathrm{B}}^{+}| \ll k_{\mathrm{A}}^{+}$, the order of magnitude of the wave speed is

$$U \approx \frac{D^{\frac{1}{2}}(k_{\mathrm{A}}^{+} - k_{\mathrm{B}}^{+})}{(k_{\mathrm{A}}^{+})^{\frac{1}{2}}} \tag{8c}$$

with a thickness $\delta \approx D^{\frac{1}{2}}/(k_{\mathrm{A}}^{+})^{\frac{1}{2}}$. This problem also has a steady spherical solution corresponding to a droplet of the stable phase imbedded in the metastable one with a radius R of order $R/\delta \approx k_{\mathrm{A}}^{+}/(k_{\mathrm{A}}^{+} - k_{\mathrm{B}}^{+})$ corresponding to an interfacial energy balancing the difference of bulk energy of A and B. However, as in nucleation theory, this solution is proved to be unstable. It is also worthwhile recalling that the solutions of (8*b*) change in nature when the upstream medium is unstable. This is the case for the problem studied by Kolmogorov, Petrovskii & Piskunov (1938) (hereinafter denoted KPP) and by Fisher (1937) represented by the following reaction rate:

$$\omega = kX(1 - X), \tag{9}$$

In this case, there is a half-infinite continuous spectrum of possible values for U, and the selected value is proved theoretically to be the lower bound, U_{KPP}, given up

$$U_{\mathrm{KPP}}/(Dk)^{\frac{1}{2}} = 2. \tag{10}$$

Here the selection mechanism is produced by the linearized production rate around the unstable state (Zeldovich 1948; Dee & Langer 1985). Such a wave can be observed only when fluctuations in the order parameter are absent from the unstable upstream medium. This is the case when the unstable upstream fluid is a lattice gas of pure species A and when the macroscopic reaction rate (9) is induced at the microscopic level by a single irreversibly reactive collision of an autocatalytic type:

$$\mathrm{A} + \mathrm{B} \xrightarrow{k} \mathrm{B} + \mathrm{B}. \tag{11}$$

The implementation of these different models on lattice gases can be done by labelling the particles, as explained in the previous section, and by changing the binary label of the particles in triple collisions (kinetic scheme, (1)) or double collisions (kinetic scheme, (11)) following rules resulting in a straightforward manner from the kinetic scheme. The collision tables differ from the ones used in the preceding section only through the colour bits. Here the reactive collisions do not conserve the number of particles of a given colour. Except for the change of colour, the collision laws are the same as in the ordinary lattice gas. The total number of particles, momentum and kinetic energy are conserved in each collision by the hydrodynamic bits. The usual continuity and Navier–Stokes equations are valid in the hydrodynamic limit and are not coupled to the chemistry of colour change controlled by the colour bits. Moreover, since the label change takes place through interactions localized at the vertices of the lattice, homogeneous equilibrium phases have no spatial correlations (perfect gas). Furthermore the mean mass fractions in the equilibrium states are given exactly by the roots of ω. Nevertheless, whenever the reverse reaction constants k^- differ from zero, the equilibrium mass fractions have Poissonian fluctuations similar to those of a perfect gas. If the kinetic coefficients k are considered to be independent of the local flow conditions, the reaction–diffusion equation (2) can be extended in a straightforward manner to the case of a non-zero velocity flow by replacing the partial derivative $\partial/\partial t$ by a Lagrangian derivative $\mathrm{D}/\mathrm{D}t$:

$$\frac{\mathrm{D}X}{\mathrm{D}t} = D\Delta X + \omega(X). \tag{12a}$$

Equation (12a) is valid in the hydrodynamic limit of small gradients, measured in mean-free-path units, and small reactive collision rates compared to the non-reactive collision rate. In the limit of a characteristic flow length A, very large compared to the front thickness δ ($\epsilon \approx \delta/A \to 0$), the local equation of evolution for a wrinkled equilibrium interface can be obtained from (12a) by using a multiscale analysis similar to the one presented by Clavin & Joulin (1983) for flames. For an equilibrium interface with a symmetric profile and constant reaction rate k (i.e. density independent), it can be shown that (see Appendix B)

$$U_\mathrm{n} = \frac{D}{R}, \tag{12b}$$

which can be written in a dimensionless form as (see (6b))

$$\frac{U_\mathrm{n}}{(kD)^{\frac{1}{2}}} = \frac{\delta}{R} + O(\epsilon^2), \quad \text{where} \frac{\delta}{R} = O(\epsilon). \tag{12c}$$

U_n and R are the normal velocity of the front relative to the flow and the radius of curvature of the front respectively. The front propagates towards the particles localized in the concave part. At the dominant order ϵ^0 of this analysis, the effect associated with the non-zero thickness of the interface dispappears and the equilibrium interface can be considered to be a passive surface in the sense that it is only convected by the flow ($U_\mathrm{n} = 0$). Curvature effects appear at the next order in the power expansion in ϵ. Notice that, contrary to the case for flames (Clavin & Joulin 1983), at this first non-trivial order ϵ^1 in the ϵ-expansion, stretching of the front by inhomogeneities in the flow field does not affect the motion of an equilibrium interface. This will no longer be true if the profile of the interface is asymmetrical as

for the generic case $k_A^+ \neq k_B^+$. In this case an additional term appears on the right-hand side of (12*b*) which involves not only the diffusion coefficient D, as in equation (12*b*), but also the reaction rate (see Appendix B). This additional term is also present when the kinetic coefficients depend on the density. We will come back to this point in the following section. In the absence of flow fields and for small amplitudes of front corrugations, (12*b*) reduces to a linear diffusion equation describing the relaxation of the front towards to a planar shape:

$$\frac{\partial \alpha}{\partial t} = D\Delta\alpha, \tag{12d}$$

where $\xi = \alpha(\eta, \zeta, t)$ is the equation for the position of the front in the frame of reference (ξ, η, ζ) where the planar front is steady and perpendicular to the ξ-axis.

However, if one wanted to describe reaction–diffusion phenomena in the absence of hydrodynamics, it is not necessary to retain momentum conservation in the collision laws controlled by the hydrodynamic bits. Another possibility could be to introduce collisions with fixed targets (wind–tree model). In the following we shall call these models without momentum conservation 'lattice diffusive gas'.

A series of computer simulations of reaction–diffusion waves have been performed with the lattice-gas model presented above:

(i) In figure 3, a sequence of pictures is presented showing the development of a planar equilibrium interface from an intitial homogeneous mixture in a computer experiment of the spinodal type. The kinetic parameters are those represented by (5). Every triple collision with particles of both colours is assumed to be reactive. This corresponds to a reaction rate, expressed in the natural units of the lattice gas, given by $k^+ = 15d^2(1-d)^4$. The density (mean number of particles per direction at each site) is $d = 0.3$. The initial condition corresponds to $X = \frac{1}{2}$ and the particles are enclosed in a two-dimensional box with periodic boundary conditions. The number of sites along Ox and Oy are the same so that the aspect ratio is $\sqrt{\frac{3}{2}}$.

A natural extension of the work presented in figure 3 concerns the mechanism of nucleation. It consists in describing the dynamics of the transition from a uniform metastable state to the thermodynamic equilibrium through a nucleation process. The procedure is similar, but the reaction constants in (3) must be chosen such that $k_A^+ \neq k_B^+$, $k_{A,B}^- \neq 0$ in such a way that there exist three different real roots of ω in the range $[0, 1]$. A slow reverse is necessary to ensure non-zero fluctuations of the order parameter X for the initial metastable state. Among the interesting features of the lattice gas model is the fact that similar numerical simulations of nucleation processes can be performed for flows in channels of arbitrary geometry without further difficulties. Among the main limitations of this simplified microscopic model is that the coupling between the kinetic constants k and the local thermodynamic conditions is only through ρ. Temperature fluctuations can be taken into account, in principle, by introducing different possible values for the modulus of the particle velocity. However such a procedure will limit the main interest of the method, which is in its characteristic of massive parallelism with a limited number of bits per site. It is easier to take into account the actual modification of local chemical equilibrium by pressure fluctuations. This can be done by prescribing a different sensitivity of the kinetic constants k^+ and k^- to the particle density. Before undertaking such a programme more simulations should be carried out to test the interest of the method.

(ii) The variation of the thickness of the equilibrium interface for the kinetic parameters represented by (5) is shown in figure 4(*a*) as a function of the inverse

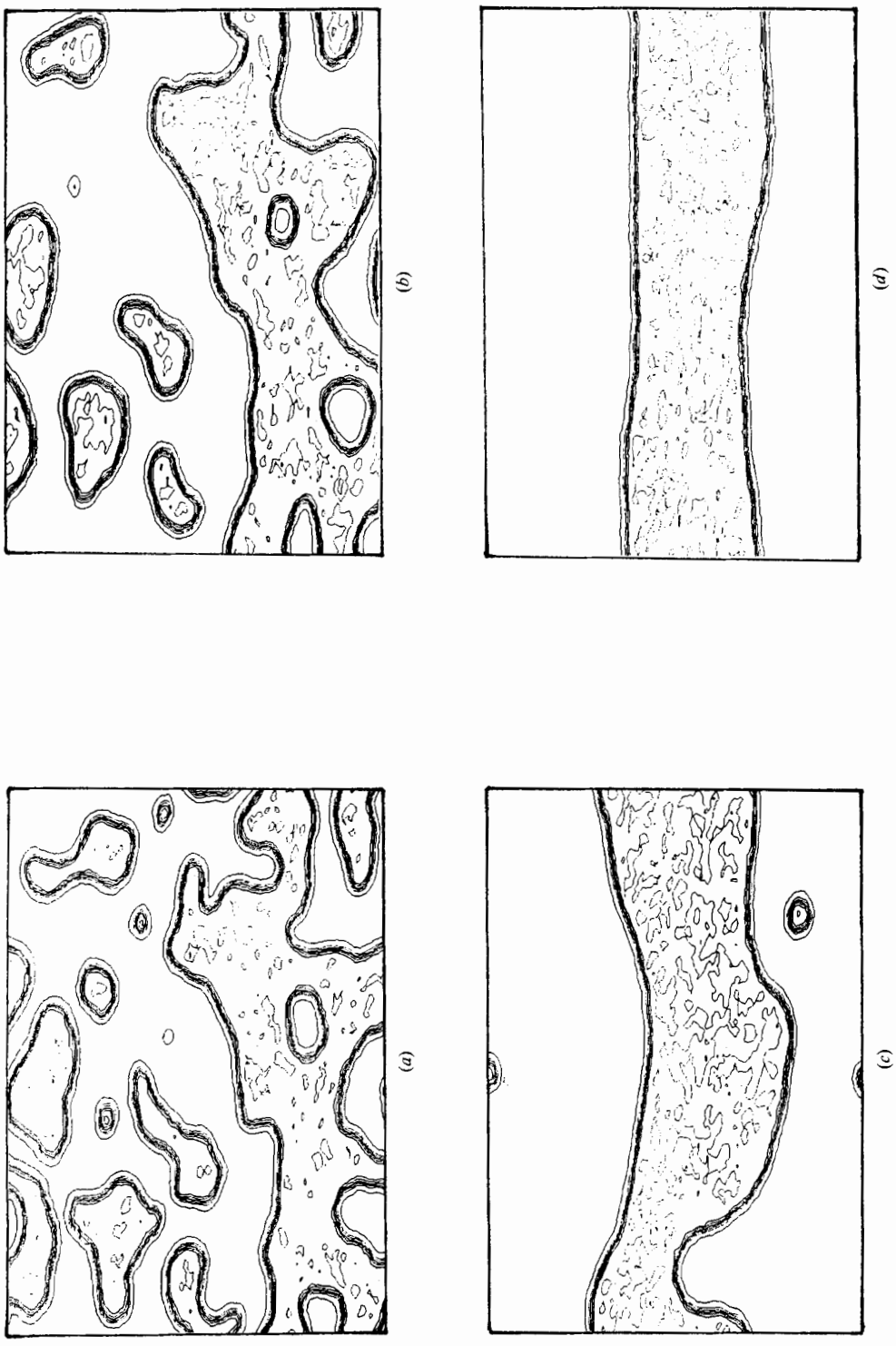

FIGURE 3. Spinodal separation of an initial homogeneous mixture in a toroidal box. (*a*) time = 200, (*b*) 400, (*c*) 1400, (*d*) 6000.

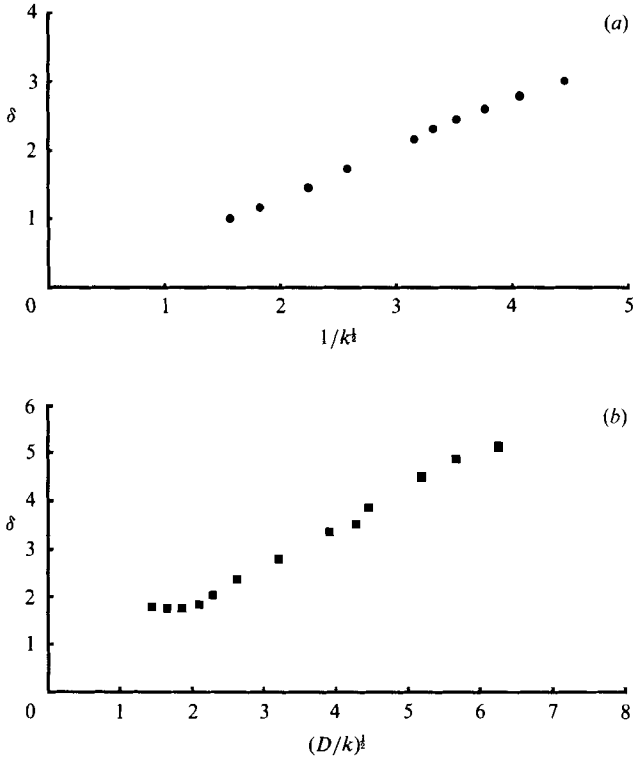

FIGURE 4. (*a*) Thickness of an equilibrium interface as a function of the square root of the inverse relaxation time; density = 0.3. (*b*) Thickness of an equilibrium interface as a function of the square root of the binary diffusion coefficient over the reaction rate.

reaction rate for constant density, $d = 0.3$, and in figure 4(*b*) as a function of diffusion coefficient over reaction rate. Each point of these curves corresponds to a different value of the reactive collision frequency controlling the colour change of the colour bits associated with triple collisions. Equation (6*b*) is found to be well verified.

(iii) The equilibrium concentrations measured on both sides of equilibrium interface are plotted in figure 5 for the symmetrical case described by (4) and for $d = 0.3$. These concentrations are found to vary with κ (the ratio of the direct and reverse reaction rates) as predicted by the theoretical values corresponding to the roots of (3).

(iv) The propagation velocity of non-equilibrium planar fronts corresponding to situations described by (8*a*) has also been measured. As shown by the results plotted in figure 6, the theoretical results of (8*c*) are well verified by the lattice-gas simulations.

(v) A direct simulation of planar KPP travelling waves described by (9) and (10) has also been carried out. The implementation on the lattice gas has been done by introducing a rule for colour change through binary collisions according to the kinetic scheme (11). Every binary collision involving two different-colour particles has been assumed to be reactive. This corresponds to a reaction rate, appearing in (9) and (10), given by $k = 6(1-d)^5 d$. The dependence of the wave speed on density thus obtained is plotted in figure 7. Agreement with (10) is found to be satisfactory only in the domain of high density. At low density the macroscopic equation (10) is no longer valid because the characteristic velocity $2(Dk)^{\frac{1}{2}}$ becomes of the order of the velocity

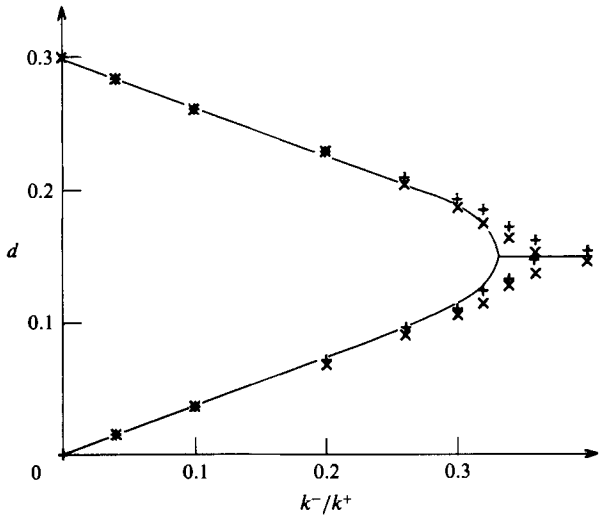

FIGURE 5. Equilibrium concentrations at a total density $d = 0.3$ as a function of the ratio of the direct to inverse reaction rates.

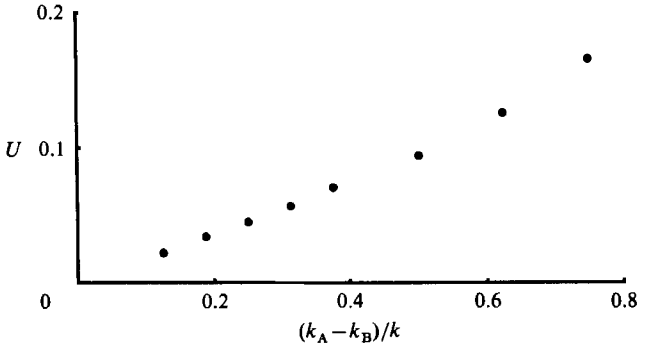

FIGURE 6. Propagation velocity of a non-equilibrium planar front as a function of the normalized difference in reaction rates.

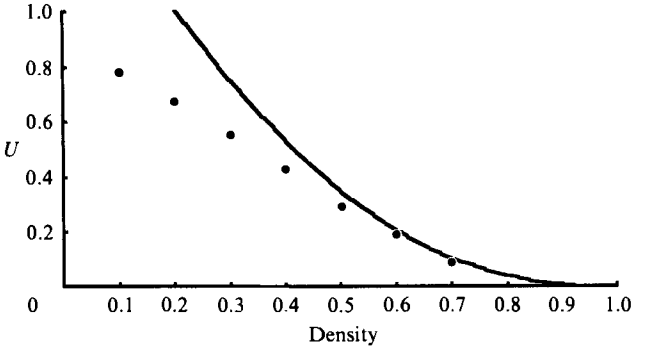

FIGURE 7. Propagation velocity of a planar KPP travelling wave as a function of density. The solid line is given by (10).

of the particles on the lattice gas (called the 'velocity of light' and equal to one in the natural units of the lattice gas). A further possible reason for discrepancy lies in the role of fluctuations, which become important at low density when the thickness of the front approaches the mean free path.

(vi) In order to check the dynamical properties of the equilibrium interface whose internal structure is described by (6*a*), we have made the following computer simulation of a forced Rayleigh type of experiment. Initially, the interface is modulated sinusoidally in a quiescent flow and its relaxation towards the planar equilibrium shape is studied. As predicted by (12*d*), the relaxation of the amplitude of modulation, shown in figure 8(*a*), is exponential in time with a relaxation rate given by $\tau^{-1} = D\ell^2$, where ℓ is the wavenumber and D the binary molecular diffusion coefficient of the mixture. The values of D measured in this computer simulation are presented in figure 8(*b*). They are slightly smaller than the binary diffusion coefficient measured in a non-reactive mixture and presented in figure 1. The accuracy could be improved by decreasing the reactive reaction rate k^+ to a value small compared with the elastic collision rate. Another type of simulation has also been carried out concerning the regression speed of a circular 'bubble' of one species imbedded in the other. As shown in figure 8(*c*), equation (12*b*) is found to be well verified. The values of the diffusion coefficient D (figure 8*b*) are a little larger than obtained from the forced Rayleigh experiment and closer to the values obtained from the binary diffusion experiments (figure 1*b*).

The model considered above has a series limitation in describing the dynamical properties of real interfaces encountered in phase transitions developing in flows: the effects of latent-heat release are neglected. In the following we shall deal with physical processes in which reaction–diffusion phenomena are coupled to thermal effects in the absence of fluid motion and which can be modelled by a 'lattice diffusive gas'. For modelling many real physical problems such as crystal growth, the order parameter X obeys a reaction diffusion equation similar to (2) but coupled (through the temperature dependence of ω) to an equation for the temperature field T associated with energy conservation:

$$\rho \frac{\mathrm{d}e}{\mathrm{d}t} = \lambda \Delta t, \tag{13}$$

where $e(X, T)$ is the enthalpy density and λ the thermal conductivity. In this frame, the rate ω is the X-derivative of a thermodynamic potential W, depending on temperature through the coefficients $k^+_{\mathrm{A,B}}$. Recent developments based on this model have been presented by Clavin (1987). At complete thermodynamic equilibrium between the two phases, the temperature is uniform such that $k^+_{\mathrm{A}} = k^+_{\mathrm{B}}$, leading to a steady planar interface ($U = 0$) as described by the solution of (5) and (6).

One possible way of introducing a temperature field into the lattice diffusive gas could be to couple the coloured lattice-diffusive-gas model to another model describing a dynamical Ising spin system (Pomeau 1984). In this model energy is conserved because spins are flipped only when they are in a zero local field. Thus to exchange energy between the spin assembly and the outside world it suffices to flip spins in a non-zero local field. Suppose for instance that one wants to bias the colour changing collisions in scheme (1) in such a way that particles A have a larger internal energy than particles B. Then one may put, on the same lattice, both moving particles and spins attached to the vertices. Choosing the internal energy difference between A and B to be exactly equal to that needed to flip a spin against the local field and correctly associating spin flipping and colour change, one may have

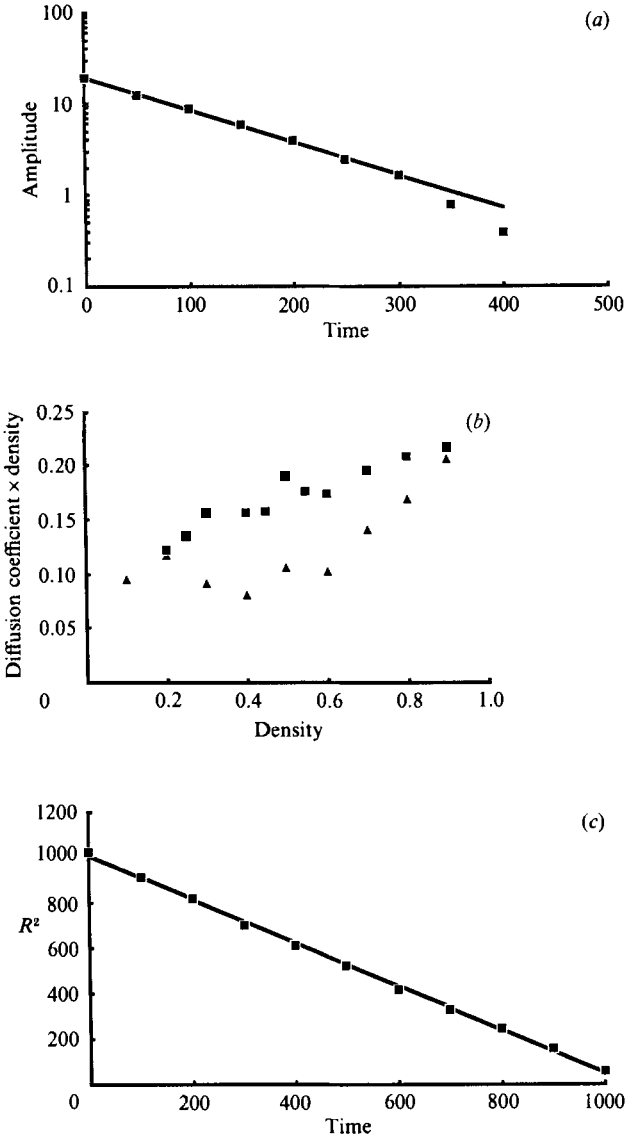

FIGURE 8. (*a*) The amplitude of an initially sinusoidal equilibrium interface as a function of time. (*b*) Diffusion coefficient times density as a function of density for the experiments of (*a*) and (*c*). (*c*) Radius squared of a circular 'bubble' (two-dimensional) with an equilibrium interface, as a function of time.

conservation of the total energy of the complete system (spin + lattice-gas particles). Thermal diffusion is ensured by the spin system with its own flipping rules, independent of particle transformation. The front motion is ensured by the 'chemistry of colours' in the lattice gas as before. The coupling to the temperature field results from the bias in the reactive collisions that are permitted only if it is possible to flip a spin attached at the corresponding site. The heat diffusion coefficient can be increased compared with the binary diffusion coefficient D by making many (sub)time steps for the spin system alone between time steps for particle collisions and colour dynamics. The infinite temperature limit is easily

understood in this representation: A and B are equally probable despite their difference of energy, and the bias in the colour change vanishes because spins parallel or antiparallel to their local field are also equally probable.

Such a model could be a good candidate to describe dentritic growth.

4. Non-miscible fluids and external gravity fields

It would be useful to be able to model interfaces between two immiscible fluids. An interesting application of this is the study of interface instabilities such as Rayleigh–Taylor or Kelvin–Helmholtz instabilities. As explained in §1, it is difficult to model complete immiscibility at the microscopic level, where it is necessary to introduce both attractive and repulsive forces. Attractive forces cannot be easily modelled in lattice gases. It is possible to imagine a collision table in which the rules concerning the colour bits are such that the interaction A–B appears to be more repulsive than the interactions A–A and B–B. However such an artifice does not seem to be sufficient to prevent diffusive mixing in a lattice gas.

In lattice-gas interface simulations one is therefore led to resort to a chemical transformation such as for the equilbrium interfaces that have been studied in §3. The problem is then to estimate the relative effect of the chemistry of colour change on the dynamics of such interfaces by comparison with the case of immiscible fluids. The two velocities to be compared are U_n, the normal velocity of the front relative to the flow, and V, the flow velocity. Since the Schmidt number is close to unity in the ordinary lattice-gas model presented in §3, the phenomenon described by (12*b*) produces an effect that is of the order of the inverse of the Reynolds number:

$$\frac{U_n}{V} \approx \frac{1}{Re}. \tag{14}$$

Two other effects must also be considered:

(i) The first one is of a general kinetic nature. It results from the fact that the conditions for thermodynamic equilibrium are not exactly satisfied because of flow inhomogeneities or because of the geometry of the front. As a result, $U_n \neq 0$. Consider, for example, pressure fluctuations produced by inhomogeneities of the flow field. From the general principles of thermodynamics, the speed of transformation is proportional to the difference of chemical potential between the two phases. From the Gibbs–Duhem relation this is proportional to the pressure fluctuation. Assuming now that the flow satisfies the Bernouilli equations, one finds that the pressure fluctuation and thus the speed of transformation of one phase into the other is proportional to the square of the liquid velocity variation. But the velocity of this front, due to the convection by the flow field, is proportional to the fluid velocity itself. Thus the ratio of the two velocities, U_n/V, is of the order of the flow velocity itself. This dimensionless ratio can only be proportional to the Mach number. Thus for ordinary subsonic flows where the Mach number is negligibly small, real interfaces, such as the liquid–vapour interface, can be considered as non-sensitive to the effects considered above. Notice that, because the kinetic coefficients $k^+_{A,B}$ depend on the local density, the lattice-gas model of §3 will probably show similar effects. In fact, the density dependence being the same for k_A and k_B, the motion of the corresponding interface is only sensitive to the effect of density change across the interface. This effect is obviously proportional to δ/R and must also increase with the Mach number. Such effects should appear in the right-hand side of (12*c*) as an

additional corrective term similar to the one for flames but involving the Mach number (Clavin & Joulin 1983).

(ii) The second effect is the modification of the local equilibrium conditions as described, for example, by the Gibbs–Thompson relation or the Laplace equation. These small effects may play a non-negligible role in the dynamics of real unstable interfaces such as in the Mullins and Sekerka instability for crystal growth or in the Rayleigh–Taylor instability. For example, they are responsible for stabilization at short wavelengths. Such phenomena are not included in the simple lattice-gas model presented in §3. In particular, the surface energy described by the first term on the right-hand side of (7*b*) is not coupled to the pressure as in the phenomena described by the Laplace equation. Nevertheless the stabilization at small wavelengths will be ensured by the phenomena described by (12*b*, *d*).

With this in mind, the equilibrium interface model presented in §3 has been used with the lattice-gas method to simulate the Rayleigh–Taylor (Rayleigh 1900; Taylor 1950) and the Kelvin–Helmholtz instabilities for which hydrodynamics is an essential mechanism. Except when explicitly specified, all the simulations have been made with $d = 0.3$ and with every triple bicoloured collision taken to be reactive.

For the Rayleigh–Taylor instability, the differential effect of gravity has been modelled by imposing that the particles belonging to one species have their momentum turned towards a given direction from time to time with a frequency proportional to the acceleration of gravity (Clavin *et al.* 1986). Because there is no difference in mass density, the effects associated with the difference in inertia are not represented. This effect of gravity is measured in dimensionless units by the ratio $\rho g\lambda/p$, where p is the pressure and λ a typical lengthscale. In our computer experiments this number remains very small. Otherwise one would leave the range of incompressible dynamics. A closed two-dimensional square box (512×512 sites) has been used. A typical curve representing the amplitude growth with time for a particle simulation is shown as an example in figure 9(*a*). The front is initially weakly wrinkled around its planar position with a wavelength equal to $\frac{1}{3}$ the length of the box. Up to 1500 time steps the amplification is found to accurately fit the theoretically result given by the dominant order of the linear theory (Taylor 1950):

$$\alpha(t) = \alpha(0)\cosh\{(g\mathscr{k})^{\frac{1}{2}}t\}. \tag{15}$$

where $\mathscr{k}$ is the corresponding wavenumber. Later in time, the nonlinear effects cannot be neglected. A typical picture after 2000 iterations and for an initial wavelength of $\frac{1}{2}$ the length of the box is presented in figure 9(*b*). The vectors represent the mass flux of one species.

The Kelvin–Helmholtz instability has first been simulated for a configuration representative of a jet using a rectangular box (1024×256 sites) with periodic boundary conditions in both directions. Initially the velocities of the fluid in the middle and on the sides are opposed with the same modulus of $\frac{3}{7}$. The total flow field and the picture of the front with the mass flux of particles in the jet are presented in figure 10(*a*) after 2000 time steps. A time series of pictures of the front is shown in figure 10(*b*). As shown on figure 10(*b*) (iii) the interaction between two interfaces leads to the formation of pockets of a single colour. These pockets then slowly regress and, because of the effect described by (12*b*), all the particles will have the same colour in the final state.

Such numerical simulations with the 14-bit lattice-gas model cannot be representive of real mixing layers because they correspond to situations in which the quantity $g(\rho)$ defined in Appendix A is not unity. In this case, a Gallilean invariant

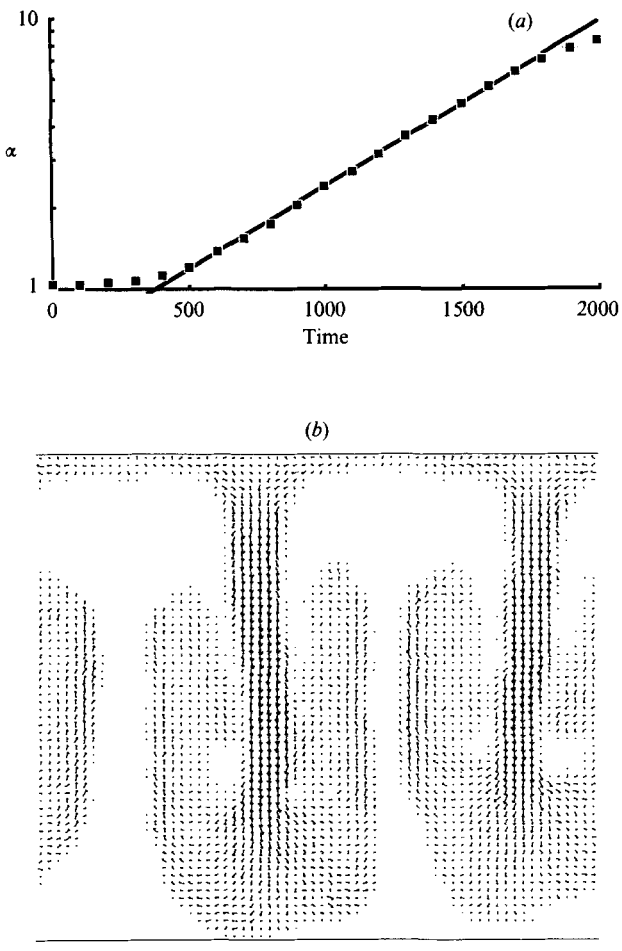

FIGURE 9. (*a*) Amplitude of an initial sinusoidal perturbation, subject to a Rayleigh–Taylor instability, as a function of time. (*b*) Mass-flux vectors for one of the species in a Rayleigh–Taylor instability at time $t = 2000$.

version ($g(\rho) = 1$ and $\mathrm{d}g/d\rho = 0$, see Appendix A) of the two-colour and reactive lattice gas must be used. As in the one-colour model presented by d'Humières, Lallemand & Searby (1987), the Gallilean invariance can be ensured by using a two-bit word to represent the population of the centres of a given colour and by biasing the non-reactive collision rules so that the mean density of the particles at rest is greater than that of the moving particles.

The corresponding 16-bit reactive lattice gas with a density/link of 0.16 and a density/site of 2.38 has been implemented on a computer to simulate the Kelvin–Helmholtz instabiliy for conditions similar to the ones that have been used in §2 but with an equilibrium interface separating the two types of particles. The kinematic shear viscosity is $\nu \approx 0.23$. The two opposed velocity vectors have the same modulus of 0.15 at the initial condition. A rectangular box (1024×256 sites) is used with stick conditions at the upper and lower boundaries and periodic conditions at the ends. The corresponding Reynolds number is $Re \approx 334$. Every triple collision with particles of both colours is assumed to be reactive so that the resulting thickness of the interface is of the order of the distance between neighbouring sites of the

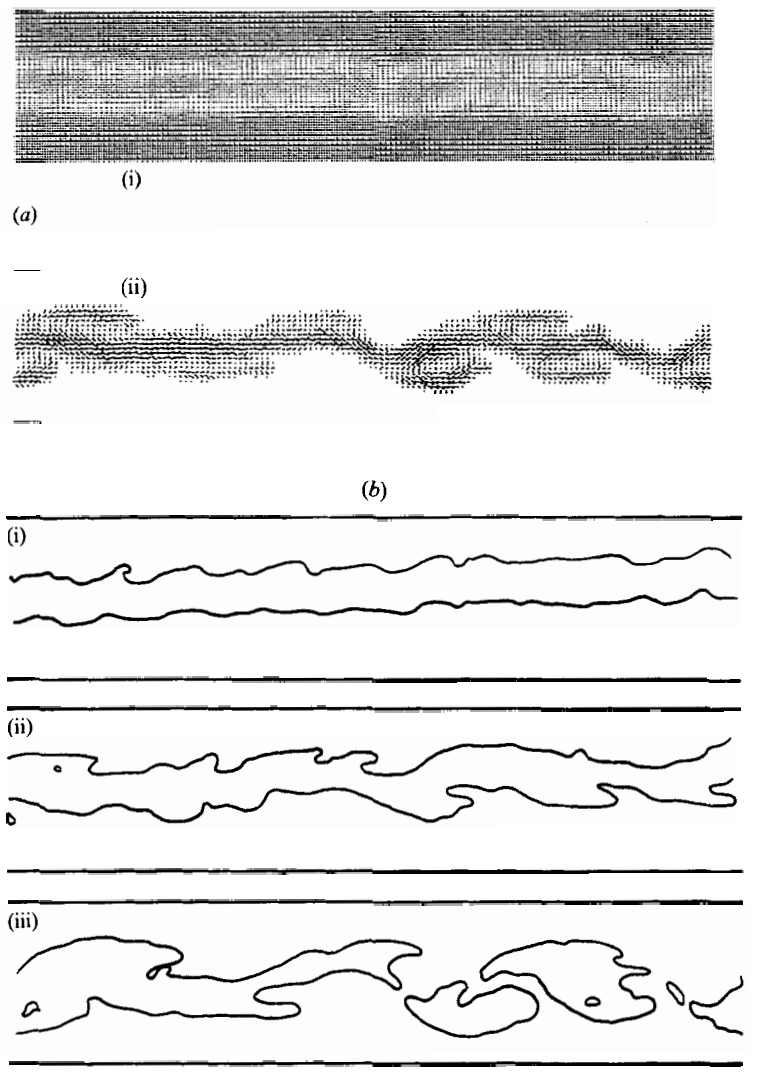

FIGURE 10. (*a*) Jet instability in a periodic channel, image taken at time = 2000. (i) Total mass flux, (ii) mass flux in the jet. (*b*) Shape of the jet at (i) time = 500, (ii) 1500, (iii) 2500.

lattice. A time series of pictures of the front is presented in figure 11(*a*). After 6000 iterations the characteristic time for the evolution of the interface becomes much longer. This results from a quasi-equilibrium at that time between the local flow field and the normal velocity of the curved front given by (12*b*). The flow field corresponding to 6000 iterations is visualized in figure 11(*b*) in which a periodic system of identical vortices which rotate in same direction is identified. The time series of figure 11(*c*) show the evolution of the isoconcentration line $X = \frac{1}{2}$ for identical conditions except that the chemical reaction is switched off so that, as in §2, molecular diffusion and turbulent mixing are the only mechanisms involved. By comparison with figure 11(*a*) this isoconcentration line and the equilibrium interface are found to have a similar shape up to 6000 iterations.

Similar simulations but with an irreversible chemical reaction $A + B \rightarrow P$ can be used in future work to study the development of a chemical reaction in turbulent

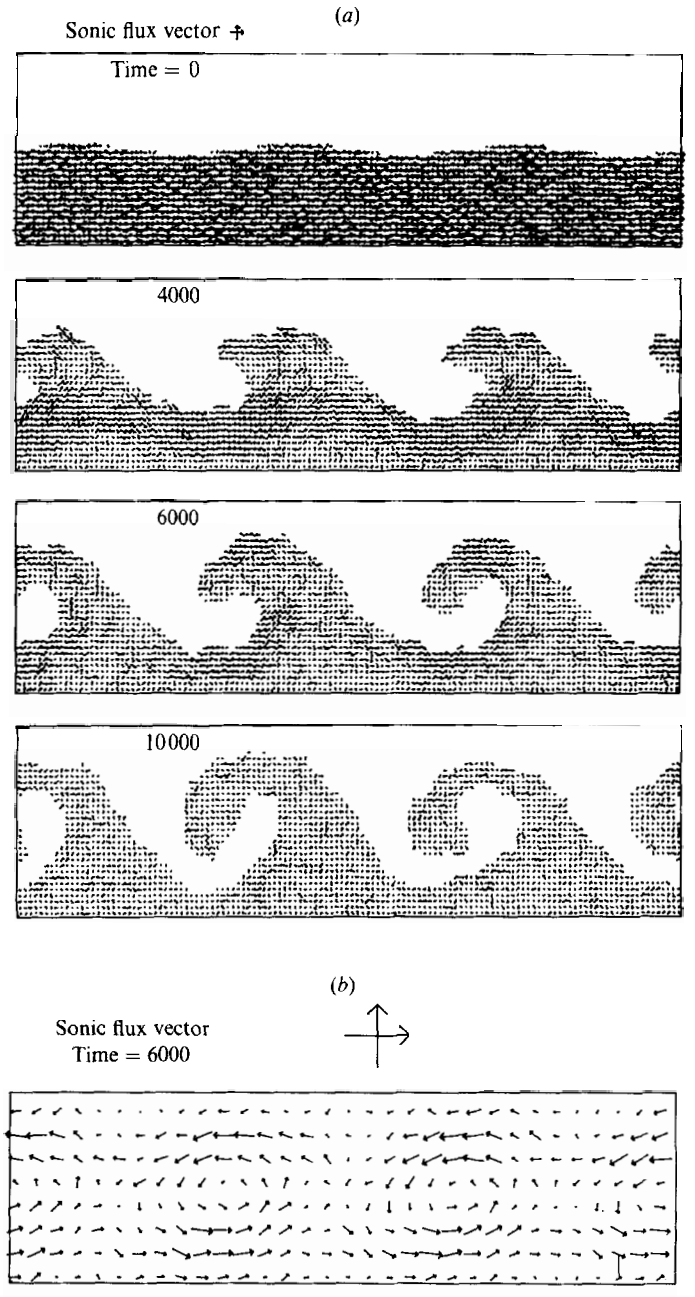

FIGURE 11 (*a*,*b*). For caption see facing page.

shear flows, in particular in two-dimensional mixing layers or axisymmetric jets. This would require the use of eight additional bits to represent the third species P. Since the corresponding reaction–diffusion sheet will behave locally like the equilibrium interface, it must present a shape similar to the one in figure 11 (*a*) as long as enough reactive species A and B are left. Such an extension of the lattice gas is particularly convenient to investigate the phenomena occurring at the small dissipative scales of the turbulent mixing layer between two reactive fluids.

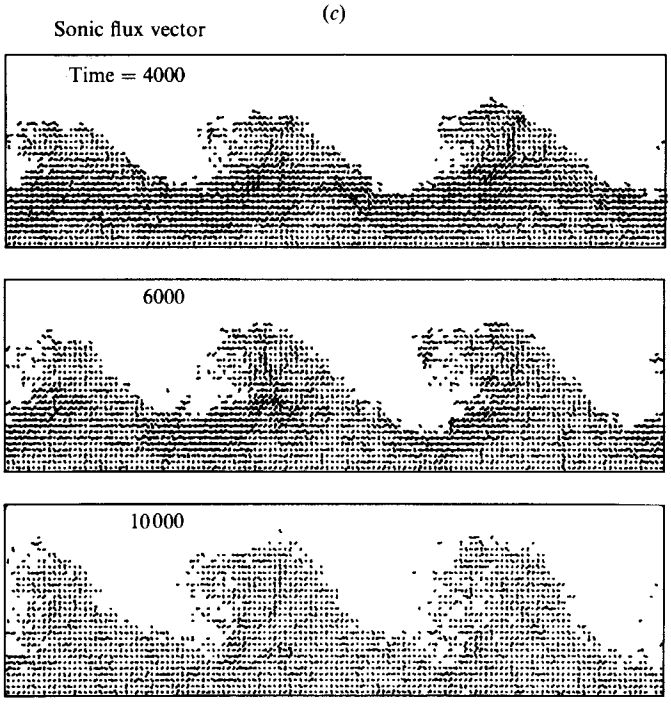

FIGURE 11. (*a*) Time series of the amplitude of an initial sinusoidal perturbation, subject to a Kelvin–Helmholtz instability. Mass fluxes of one species are shown with averaging over, 8×8 sites during 16 times steps. (*b*) Flow field at time = 6000. Total mass fluxes are shown with averaging over 16×16 sites during 16 times steps. (*c*) Time series of a mixing layer corresponding to the same conditions as in (*a*) but without the equilibrium interface. Mass fluxes of one species are plotted with the conditional sampling $X \geqslant \frac{1}{2}$. Same averaging as in (*a*) is used.

A more simple extension would be to use the 16-bit lattice-gas model with a similar interface model but with $k_A^+ \neq k_B^+$ in order to represent a reaction front, such as a premixed flame, propagating with a non-zero normal burning velocity (given by (8*c*) in the planar case) in a shear flow. Modifications of the burning rate by stretching and by wrinkling of the front will be well represented but such a simple model will be unable to describe the hydrodynamical effects associated with the difference of density. A model for a two-density flow is presented in the following section.

5. Flame fronts

Flames present two major differences from the fronts studied so far. First, chemical processes involved in flames are always far from equilibrium and are not related to any phase coexistence at thermodynamic equilibrium. Secondly, in the non-planar case, the isobaric coupling between thermal effects and hydrodynamics plays a dominant role notably through the Darrieus–Landau instability (G. Darrieus 'Propagation d'un front de flamme', unpublished work presented at *La Technique Moderne*, 1938, and *Le Congrés de Mécanique* Appliquée, Paris 1945; Landau 1944). For a recent review see Clavin (1985). The flame front separates two gas flows of different mass density ($\rho_u > \rho_b$) and propagates in the frame of the unburnt mixture at a flame speed U_u much smaller than the sound velocity C_u (small-Mach-number approximation, $M = U/C \ll 1$). The subscripts u and b refer to unburnt and burnt

mixtures respectively. In the approximation $M \ll 1$, the molecular density n is related to the temperature T through an isobaric approximation $n_u T_u = n_b T_b$. In the frame of the flame front, the velocity components of the unburnt and burnt gas flows normal to the front, U_u and U_b, are related by the mass conservation equation, $\rho_u U_u = \rho_b U_b$.

The purpose of this section is to present an extension to the lattice-gas model that could be used to simulate some typical problems of flames such as the Darrieus–Landau hydrodynamic instability, curved flame fronts propagating in tubes (Zeldovich *et al.* 1980; Pelcé 1985) or the coupling with acoustic phenomena.

From the basic physics involved in flames at the molecular level, unburnt cold reactive species must be transformed irreversibly into burnt hot ones. Therefore the lattice-gas model must contain particles with two different kinetic energies at least. This necessitates the introduction of important modifications into the original isothermal lattice-gas model. The model proposed here contains two different sorts of particles: unburnt and burnt. The unburnt particles have a unit velocity modulus and a mass equal to two. The burnt ones have a unit mass and a velocity modulus equal to two. Thus the modulus of the momentum is the same for all the particles but the burnt ones have a kinetic energy two times larger than the unburnt ones, and as a consequence the temperature ratio T_b/T_u is equal to two and the mass density ratio ρ_u/ρ_b is equal to four. The two kinds of particles move on the same hexagonal lattice and the collision laws between identical particles are the same as those in the original isothermal one-species lattice-gas model. Since the two species have the same value for the modulus of the momentum, the laws for elastic collisions involving burnt and unburnt particles are also the same as the original collision laws. These collisions are necessary to equalize the pressure of the burnt and unburnt mixtures so that the molecular and mass density ratios are two and four respectively. The exothermal irreversible chemical reaction is modelled by the splitting of a single unburnt particle into two burnt ones, compatible with momentum conservation. The thermal feedback can be represented by an autocatalytic process similar to the one described above: the splitting reaction is conditioned by the presence of a sufficiently large proportion of burnt neighbouring particles (multiple collisions). To minimize compressibility effects associated with the finite Mach number and also to smooth out the spurious transient increase in molecular density produced locally by each splitting reaction, one must decrease the splitting rate sufficiently compared with the elastic collision rate. The flame thickness δ is thus necessarily much larger than the mean free path, as in real flames. In practice this means that simulations of cases corresponding to very large Reynolds numbers, $Re \approx L/\delta$, make very heavy demands on computer memory and execution time. In the lattice-gas model with two velocity moduli, the thermal diffusivity is identical with the binary molecular diffusion coefficient and thus the Lewis number is unity.

Much work remains to be done to determine theoretically the correct macroscopic equations corresponding to this lattice-gas model. But the preliminary simulations are very encouraging. In particular, in simulations of unsteady flame propagation in a closed vessel, the generation of acoustic and shock waves propagating back and forth has been clearly exhibited. The transition to detonation has also been observed. Flame propagation in an open channel (1024×256 sites) with periodic conditions at the sidewalls has also been simulated. In these conditions the appearance of cellular flames created by the hydrodynamic instability has been observed and is presented in figure 12. The initial condition is a planar flame and the uniform flow velocity of the reactant is adjusted to be the same as the flame speed in order to keep the position of the flame front stationary (figure 12*a*). After 1200 times steps, strongly

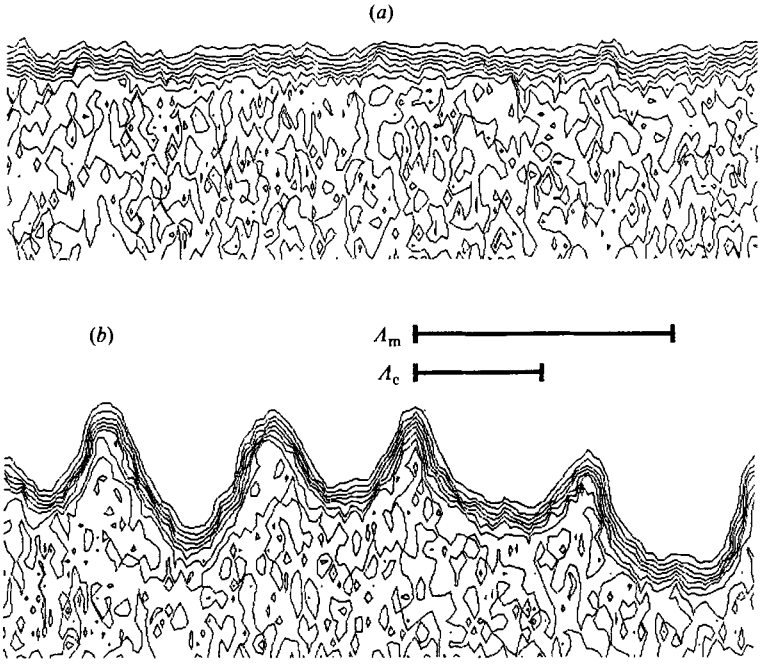

FIGURE 12. Propagation of a premixed flame with heat release, showing the Darrieus–Landau instability. The lines are isoconcentration contours. The unburnt species enter at the bottom. (*a*) time = 100 (*b*) 1200. The marginally stable wavelength Λ_c and the most unstable one Λ_m evaluated from Clavin (1985) equations (52) and (78*b*) are also shown in this figure. The numerical values used in these equations are those corresponding to the conditions of this simulation: gas expansion coefficient $\gamma = 0.75$, Lewis number $Le = 1$, flame speed $u_L = 0.05$ and thermal diffusivity $D_{th} = 0.35$. Λ, u_L, and D_{th} are measured in the natural units of the lattice gas.

nonlinear cells are clearly observed (figure 12*b*). The characteristic size of these cells is observed to be of the same order of magnitude as the marginally stable wavelength predicted by the theoretical analysis (Pelcé & Clavin 1982; Clavin 1985). The isoconcentration lines of reactants are plotted in these figures. The Mach number ($M_u \approx 10^{-1}$) of the flame modelled here by the lattice-gas method is not very small and the coupling with acoustic modes is strong when compared with real flames ($M_u \approx 10^{-3}$). One thus has to be careful when the developing of the above numerical simulations that compressibility effects, responsible for the interaction between flame and pressure waves, do not hide the hydrodynamic instability.

6. Conclusions and prospects

It has been shown that the dynamics of a large variety of fronts in flows can be represented by an extension of lattice-gas models with two different types of particles. This requires a number of bits per site of the order of twice that of the initial model. This method presents the advantage of simplicity and flexibility of the software. Three-dimensional simulations are currently in process. At the present time, the CPU time is similar to that needed by the more classical numerical methods. The advent of special purpose computers based on cellular automata taking full advantage of the Boolean character of the particles as well as of the natural parallelism of the method will open new horizons.

Much remains to be accomplished, especially in the theoretical analysis, to

improve the basic algorithms presented in this paper and more particularly in the representation of phase transitions and combustion phenomena. This method is presently limited to flows having moderate Reynolds and Mach numbers. Progress in this direction can be expected in the near future. This method cannot easily handle the complex chemistry occurring in combustion, but the basic propagation mechanisms as well as hydrodynamic and acoustic phenomena are well described and this new method could be very useful in the study of some important aspects of instabilities developing in industrial combustion chambers. Moreover this method appears also to be very convenient in the study of reactive mixing layers.

We thank Bruno Denet for his help in the numerical simulations. This work was supported in part by E.E.C. contract no. ST2J-0029-F, D.R.E.T. contract no. 86/1359 and C.N.R.S.-GRECO 70.

Appendix A. Basic lattice-gas dynamics

The lattice-gas model proposed by Frisch *et al.* (1986) involves Boolean particles located at the vertices of a regular hexagonal lattice of unit cell length. The particles have velocities $\boldsymbol{c}_i$ of unit modulus and point in one of the 6 possible directions corresponding to the links between one node of the lattice and its six nearest neighbours. At each time step these particles 'propagate' synchronously from vertex to vertex where they may undergo collisions with other particles. The Boolean model excludes the possibility of two particles occupying the same vertex with the same velocity, so the state of a vertex is completely described by six binary digits. The basic collision rules between the particles are given in figure 13(a, b). d'Humières & Lallemand (1986) have shown that it is advantageous to introduce a seventh stationary particle (having an internal energy) that can be created or destroyed by the momentum-conserving collisons of figure 13(c, d). The presence of these stationary particles significantly increases momentum redistribution, reducing viscosity and increasing the maximum attainable Reynolds number for a given lattice. Define the macroscopic quantities

$$\text{total density} \quad \rho = \sum_{i=1}^{7} n_i, \tag{A 1}$$

$$\text{total flux} \quad \rho \boldsymbol{u} = \sum_{i=1}^{7} n_1 \boldsymbol{c}_1, \tag{A 2}$$

where n_i represents one of the 7 possible particles at a vertex. Note that the macroscopic ρ used in this Appendix is not the same as the microscopic density ($d = \rho/7$) used in the body of the paper. It has been shown (Frisch *et al.* 1986; Rivet & Frisch 1986) that, with suitable limits, these macroscopic quantities satisfy the continuity equation

$$\frac{\partial \rho}{\partial t} + \boldsymbol{\nabla} \cdot (\rho \boldsymbol{u}) = 0, \tag{A 3}$$

and a Navier-Stokes equation

$$\frac{\partial (\rho u_\alpha)}{\partial t} + \sum_\beta \frac{\partial}{\partial x_\beta} (\rho g(\rho) u_\alpha u_\beta) = -\frac{\partial p}{\partial x_\alpha} + \eta_1 \nabla^2 u_\alpha + \eta_2 \frac{\partial (\boldsymbol{\nabla} \cdot \boldsymbol{u})}{\partial x_\alpha}, \tag{A 4}$$

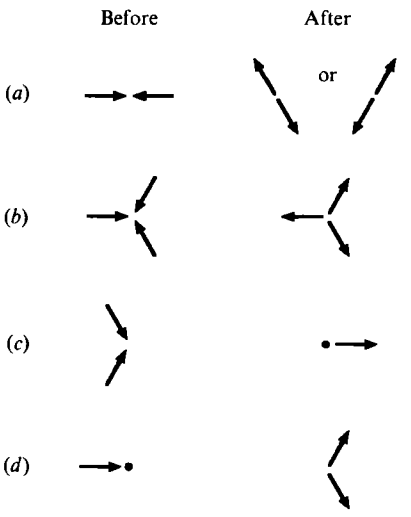

FIGURE 13. Basic collision rules for a lattice gas conserving particle number and momentum. (*a*) two-body collision; (*b*) three-body collision; (*c*) and (*d*) creation and destruction of stationary particles. Further three-body collisions can be constructed from the two-body collisions plus a 'spectator', four- and five-body collisions can be obtained by hole–particle inversion from the three- and two-body collisions respectively, leading to a total of 76 possible non-transparent collisions among the 2^7 possible precollision states.

where $\eta_1(\rho)$ and $\eta_2(\rho)$ are the shear and bulk viscosities respectively. The equation of state for the pressure is given by

$$p = \tfrac{3}{7}\rho \tag{A 5}$$

and in the natural units of the lattice gas the speed of sound is

$$C = (\tfrac{3}{7})^{\frac{1}{2}}, \tag{A 6}$$

which is close to the maximum speed for the transfer of information on the lattice ('speed of light').

It should be noted that the nonlinear convection term in the Navier–Stokes equation contains an unusual density-dependent factor:

$$g(\rho) = \frac{7}{12}\frac{(7-2\rho)}{(7-\rho)}, \tag{A 7}$$

which is not equal to unity. The standard Navier–Stokes equation can be obtained in the incompressible limit ($g(\rho)$ constant) by dividing (A 4) by $g(\rho)$ and absorbing this factor in a non-homogeneous rescaling of time, pressure and viscosities. The effective Reynolds number is also rescaled:

$$Re = \frac{ul\rho g(\rho)}{\eta_1}. \tag{A 8}$$

d'Humières *et al.* (1987) show that it is possible to obtain a lattice gas for which $g(\rho) = 1$ and $\partial g(\rho)/\partial\rho = 0$ at some particular density. This is done by using a two-bit word to represent the population of the stationary particles at a vertex and by

biasing the collision rules for the creation and destruction of these particles so that the equilibrium population is greater than that of the moving particles. An extension to three-dimensional lattice gases has also been done (Clavin *et al.* 1986).

Appendix B.

The purpose of this Appendix is to prove that (12*b*) is valid for equilibrium interfaces whose structure is symmetrical.

In the reference frame moving with the wrinkled front, the dimensionless equation for the evolution of the mass fraction X yields (see (12*a*))

$$\frac{\partial X}{\partial \tau}+\left(m+\frac{\partial^2 a}{\partial y^2}\right)\frac{\partial X}{\partial x}+v\frac{\partial X}{\partial y}-2\frac{\partial a}{\partial y}\frac{\partial^2 X}{\partial x\,\partial y}=\left(1+\left|\frac{\partial a}{\partial y}\right|^2\right)\frac{\partial^2 X}{\partial x^2}+\frac{\partial^2 X}{\partial y^2}+\omega(X), \tag{B 1}$$

where

$$m=u-\frac{\partial a}{\partial t}-v\frac{\partial a}{\partial y}, \tag{B 2}$$

$$a=\frac{\alpha(\eta,t)}{d} \tag{B 3}$$

is the reduced position of the front, and

$$x=\frac{\xi-\alpha}{d},\quad y=\frac{\eta}{d},\quad \tau=tk \tag{B 4}$$

are the reduced coordinates.

$$u(\epsilon(x+a),\epsilon y,\epsilon\tau),\quad v(\epsilon(x+a),\epsilon y,\epsilon\tau) \tag{B 5}$$

are the ξ- and η-components of the dimensionless flow velocity, reduced by $(Dk)^{\frac{1}{2}}$. When the characteristic variation length of the flow is assumed to be large compared with the thickness of the interface, $\epsilon=(\delta/\Lambda)$ is a small number. If $u=O(1)$, $v=O(1)$ one may look for the solution in a power expansion with ϵ as the small parameter:

$$\left.\begin{aligned} a&=\epsilon^{-1}a_0(\epsilon y,\epsilon\tau)+a_1(\epsilon y,\epsilon\tau)+O(\epsilon)\\ m&=m_0(\epsilon x,\epsilon y,\epsilon\tau)+\epsilon m_1(\epsilon x,\epsilon y,\epsilon\tau)+O(\epsilon^2),\\ X&=X_0(x,\epsilon y,\epsilon\tau)+\epsilon X_1(x,\epsilon y,\epsilon\tau)+O(\epsilon^2).\end{aligned}\right\} \tag{B 6}$$

The following integral relation is obtained by an x-integration of (B 1) times $\partial X/\partial x$:

$$\int_{-\infty}^{\infty}\frac{\partial X}{\partial\tau}\frac{\partial X}{\partial x}\mathrm{d}x+\int_{-\infty}^{+\infty}\left\{m+\frac{\partial^2 a}{\partial y^2}\right\}\left(\frac{\partial X}{\partial x}\right)^2\mathrm{d}x+\int_{-\infty}^{+\infty}v\frac{\partial X}{\partial y}\frac{\partial X}{\partial x}\mathrm{d}x$$
$$-\frac{\partial a}{\partial y}\frac{\partial}{\partial y}\int_{-\infty}^{+\infty}\left(\frac{\partial X}{\partial x}\right)^2\mathrm{d}x=\int_{-\infty}^{+\infty}\frac{\partial^2 X}{\partial y^2}\frac{\partial X}{\partial x}\mathrm{d}x+\int\omega(X)\,\mathrm{d}X. \tag{B 7}$$

Equation (B 7) is simpler for an equilibrium interface because the last term on the right-hand side is zero.

At the dominant order ϵ^1 of the expansion, the solution of (B 1) is

$$m_0\left(1+\left|\frac{\partial a_0}{\partial y}\right|^2\right)^{-\frac{1}{2}}=U_L,\quad X_0=X_L(x_n), \tag{B 8}$$

with $x_n = x(1+|\partial a_0/\partial y|^2)^{-\frac{1}{2}}$ and where U_L and X_L are the solutions of (8*b*) written in a dimensionless form.

In the case of an equilibrium interface, one has

$$\int \omega(X)\,\mathrm{d}X = 0 \Rightarrow U_L = 0 \Rightarrow m_0 = 0 \Rightarrow (U_n)_0 = 0. \tag{B 9}$$

If in addition $\omega(X)$ is symmetrical around $X = \frac{1}{2}$, one has

$$\int_{-\infty}^{+\infty} x_n \left(\frac{\mathrm{d}X_L}{\mathrm{d}x_n}\right)^2 \mathrm{d}x_n = 0 \Rightarrow \int_{-\infty}^{+\infty} x \left(\frac{\partial X_0}{\partial x}\right)^2 \mathrm{d}x = 0, \tag{B 10}$$

where the origin of the x-axis is choosen at the inflexion point of the X_0 profile. The first non-trivial-order term in the ϵ-expansion of (B 1) and (B 7) involves terms such as $\partial X_0/\partial\tau$ and $\partial X_0/\partial y$ which, according to (B 8), are proportional to $x\partial X_0/\partial x$. According to (B 10), the first and third terms on the left-hand side of (B 7) must vanish at this order in ϵ. For the same reason, those first-order terms in m_1 which include gradients of the flow velocity coming from the expansion of (B 5), give a zero contribution to (B 7), which reduces to

$$\left\{m_1(x=0) + \frac{\partial^2 a_0}{\partial y^2}\right\}\left(1+\left|\frac{\partial a_0}{\partial y}\right|^2\right)^{-\frac{1}{2}} + \frac{\partial a_0}{\partial y}\frac{\partial}{\partial y}\left(1+\left|\frac{\partial a_0}{\partial y}\right|^2\right)^{-\frac{1}{2}} = 0, \tag{B 11}$$

where the following relation has been used (see (B 8):

$$\int_{-\infty}^{+\infty} \left(\frac{\partial X}{\partial x}\right)^2 \mathrm{d}x = \left(1+\left|\frac{\partial a_0}{\partial y}\right|^2\right)^{-\frac{1}{2}} \int_{-\infty}^{+\infty} \left(\frac{\mathrm{d}X_L}{\mathrm{d}x_n}\right) \mathrm{d}x_n. \tag{B 12}$$

By noticing that $\epsilon m_1(x=0)\{1+|\partial a_0/\partial y|^2\}^{-\frac{1}{2}}$ reduces to $(U_n)_1/(Dk^2)^{\frac{1}{2}}$, (B 9) and (B 12) yield the result of (12*b*, *c*).

When the X-profile is not symmetrical, (B 10) is not verified and an additional term $\boldsymbol{n}\cdot\boldsymbol{\nabla u}\cdot\boldsymbol{n}$ will appear on the right-hand side of (12 b, c) ($\boldsymbol{u}$ and $\boldsymbol{n}$ are the flow velocity at the front and the unit vector normal to the front respectively), see Clavin & Joulin 1983. This term describes stretching of the front by inhomogeneities in the flow at the front. Notice that for dimensional reasons, such a term makes U_n a function of the reaction rate k (through the thickness of the interface δ) and, not only of the binary diffusion coefficient D as in (12*b*).

REFERENCES

Barrenbaltt, G. I. & Zeldovich, Ya. B. 1972 *Ann. Rev. Fluid. Mech.* **4**, 285.

Boyer, L. 1980 *Combust. Flame* **39**, 321.

Cahn, J. W. & Hilliard, J. E. 1959 *J. Chem. Phys.* **31**, 688.

Clavin, P. 1985 *Prog. Energy Combust. Sci.* **11**, 1.

Clavin, P. 1987 Kinetic effects on the dynamics of diffuse interfaces *PCH Conference, La Rabida, NATO ASI Series*. Plenum.

Clavin, P., d'Humières, Lallemand, P. & Pomeau, Y. 1986 *C.R. Acad. Sci. Paris* **303**, 1169.

Clavin, P. & Joulin, G. 1983 *J. Phys. Lett.* **44**, L1.

Dee, G. & Langer, J. S. 1985 *Phys. Rev. Lett.* **50**, 383.

Fisher, R. A. 1937 *Ann. Eugenics* **7**, 355.

Frisch, U., Hasslacher, B. & Pomeau, Y. 1986 *Phys. Rev. Lett.* **56**, 1505.

Hardy, J:, de Pazzis, O. & Pomeau, Y. 1976 *Phys. Rev.* **A 13**, 1949.

HARDY, J. & POMEAU, Y. 1972 *J. Math. Phys.* **13**, 1042.

HARDY, J., POMEAU, Y. & DE PAZZIS, O. 1973 *J. Math. Phys.* **14**, 1746.

D'HUMIÈRES, D., FRISCH, U. & LALLEMAND, P. 1986 *Europhys. Lett.* **2**, 291.

D'HUMIÈRES, D. & LALLEMAND, P. 1986 *Physica* **140A**, 337.

D'HUMIÈRES, D., LALLEMAND, P. & SEARBY, G. 1987 *Proc. Santa Fe conference on Large Physical Systems*. Complex Systems, vol. 1, p. 633.

D'HUMIÈRES, D., POMEAU, Y. & LALLEMAND, P. 1985 *C.R. Acad. Sci. Paris* **301**, 1391.

KOLMOGOROV, A. N., PETROVSKII, I. G. & PISKUNOV, N. S. 1938 *Bjul. Moskovskovo Gos. Univ.* **1**, No. 7, 1.

LANDAU, L. 1944 *Acta Physicochemica USSR* **19**, 77.

PELCÉ, P. 1985 *J. Phys. Paris* **46**, 503.

PELCÉ, P. & CLAVIN, P. 1982 *J. Fluid Mech.* **124**, 219.

POMEAU, Y. 1984 *J. Phys.* **A17**, L-415.

RAYLEIGH, LORD 1900 *Scientific Papers* vol. II, 200.

RIVET, J. P. & FRISCH, U. 1986 *C.R. Acad. Sci Paris* **302**, 267.

ROSHKO, A. 1967 *AIAA J.* **14**, 1349.

TAYLOR, G. I. 1950 *Proc. R. Soc. Lond.* **A201**, 192.

ZELDOVICH, YA. B. 1948 *Zhur. Fiz. Khim. USSR*, **22**, 27.

ZELDOVICH, YA. B., ISTRATOV, A. G., KIDIN, N. I. & LIBROVICH, V. B. 1980 *Combust. Sci. Technol.* **24**, 1.